Impact of Synchronization on Performance of Enhanced Array-Receivers in Wideband CDMA Networks

Karim Cheikhrouhou, Sofiène Affes, *Member, IEEE*, and Paul Mermelstein, *Fellow, IEEE*

***Abstract*—Synchronization performance of the receivers may severely impact the capacity or spectrum efficiency of wideband code division multiple access (CDMA) networks. Evaluations of uplink capacity for improved spatio–temporal array receivers (STAR) and the two-dimensional RAKE (2-D-RAKE) with both perfect and active synchronization indicate that synchronization with the early–late gate component of a RAKE-type receiver may constitute a bottleneck to performance improvement. Enhancement of synchronization remains a key issue. Results also suggest that STAR offers a promising alternative to the 2-D-RAKE with early–late gate, offering an average increase in spectrum efficiency up to 100% in the presence of synchronization errors at both data rates of 9.6 and 128 Kb/s. This gain further increases in high Doppler and fast multipath delay drifts. Data oversampling above the chip-rate favors STAR even more. Significant simplifications are introduced in the formulation of the STAR receiver which result in complexity comparable to the 2-D-RAKE.**

***Index Terms*—Acquisition, eigen-subspace tracking, space–time processing, time-delay synchronization, tracking.**

I. Introduction

ENHANCEMENTS in receiver operation for cellular code division multiple access (CDMA) systems, e.g., signal combining, power control, or channel coding, have led to increases in cell capacity and spectrum efficiency and are now included in proposed standards for third-generation wireless systems [1]. However, such high-capacity operation requires synchronization at significantly reduced SNR levels. Synchronization with the conventional RAKE, which relies on the early–late gate [2], may seriously limit the SNR. Previous works assessing capacity assuming perfect synchronization may provide overoptimistic results. We study the impact of practical synchronization requirements on blind[1] receiver structures using antenna arrays to estimate the possible performance degradations.

Among the blind space–time array processors selected for assessment, we consider the two-dimensional RAKE (2-D-RAKE) [4]–[6], a representative of a family of array-receivers based on the "RAKE technology." Utilization of the RAKE requires a combination of its finger outputs and suggests that the synchronization step involved in extracting those outputs is perfect, even though synchronization errors are expected in practice. In situations where degradations due to imperfect synchronization are of interest, evaluation of the RAKE performance requires inclusion of the early–late gate [2], [7]. Extension of the early–late gate to match the space–time array-processing capabilities of the 2-D-RAKE and evaluation of its performance represents one of the contributions of this paper.

We have recently presented a new receiver structure [8], the spatio–temporal array receiver (STAR),[2] which promises very rapid and accurate synchronization of multipath in the presence of slow or fast Doppler. Such high performance is obtained at the cost of a high computational load for synchronization. Comparative evaluation of STAR and the 2-D-RAKE, both in terms of performance and complexity, is of great interest. An additional contribution of this paper is the reduction in complexity of the acquisition module in STAR while maintaining the synchronization accuracy at its current level. We also propose a far more stable and accurate procedure for tracking the number of multipaths. Finally, we introduce slow channel identification update and develop a partially despread version of STAR to further reduce the complexity of the tracking module in a manner similar to [10].

The organization of this paper is as follows: In Section II, we explain the data model and the assumptions made therein, then briefly review the receiver structures of the 2-D-RAKE and STAR. We develop alternative improved versions of the early–late gate for operation with the 2-D-RAKE. In Section III, we introduce synchronization enhancements that reduce complexity and enhance performance in both steps of multipath acquisition and tracking of STAR. In Section IV, we describe the system-level evaluation tool we have developed and report on the impact of synchronization on performance as a function of design variables and operating conditions. We consider the effect of the antenna-array dimension, the case of fast channel

Manuscript received February 1, 2001; revised June 28, 2001. This work was supported by the Bell/Nortel/NSERC Industrial Research Chair in Personal Communications and by the NSERC Research Grants Program. This paper was presented in part at the IEEE Conferences Asilomar'2000, Pacific Grove, CA, October 29–November 1, 2000, and Asilomar'2001, Pacific Grove, CA, November 4–7, 2001.

K. Cheikhrouhou is with École Nationale d'Ingénieurs de Tunis, Tunis, 1002, Tunisia. He is currently on leave at INRS-Télécommunications, Université du Québec, Montréal, QC, H5A 1C6, Canada (e-mail: cheikhro@inrs-telecom.uquebec.ca).

S. Affes and P. Mermelstein are with INRS-Télécommunications, Université du Québec, Montréal, QC, H5A 1C6, Canada (e-mail: affes@inrs-telecom.uquebec.ca; mermel@inrs-telecom.uquebec.ca).

Publisher Item Identifier S 0733-8716(01)10295-7.

[1]The practical interest of blind receivers in wireless communications is well underlined in [3].

[2]A semi-blind pilot-assisted version of STAR was suggested in [9] without active synchronization. Incorporation of timing and assessment of its impact on performance of this version will be addressed in a future work.

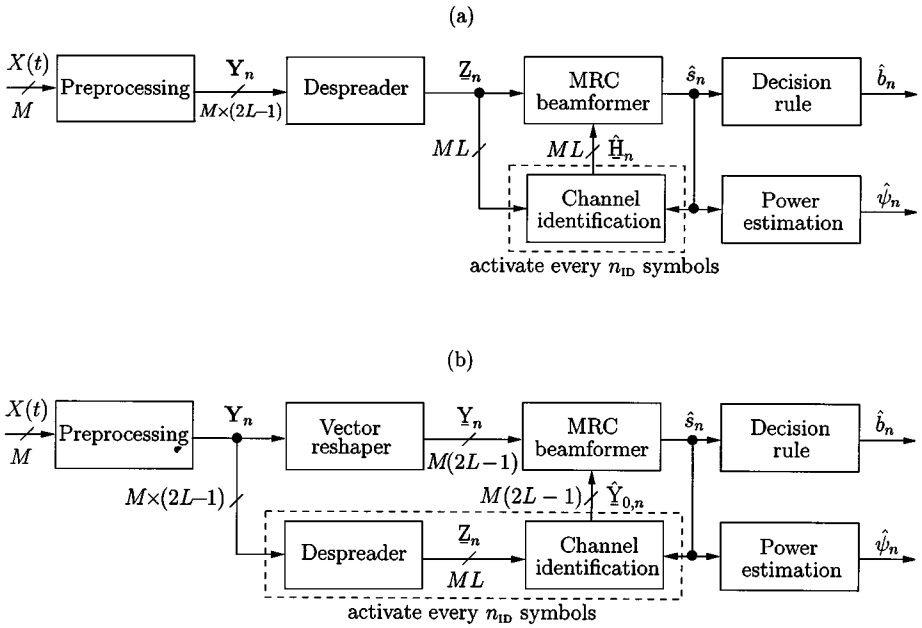

Fig. 1. Block diagram of STAR receiver with MRC implemented (a) after despreading and (b) before despreading.

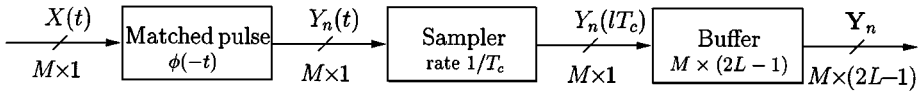

Fig. 2. Block diagram of the preprocessing unit in STAR.

parameter variations, the impact of pulse rolloff selection and of pulse waveform distortions. Section V reports the significant conclusions, namely the reduced sensitivity of STAR to synchronization errors as compared to the 2-D-RAKE.

II. Formulation and Background

A. Data Model

We consider a single-user receiver structure on the uplink direction (portable-to-base station) of a cellular CDMA system. Extension to downlink scenarios is similar, irrespective of whether the portable terminals are equipped with one or more receive antennas. Let us assume that each base station is equipped with M receiving antennas. We consider P propagation paths in a selective fading multipath environment where the time-delay spread $\Delta\tau$ is small compared to T. The user phase shift-keying symbol sequence, binary or quaternary, is first differentially encoded at a rate $1/T$, where T is the bit duration. The resulting sequence $b(t)$ is then spread with a long binary pseudorandom noise sequence $c(t)$ at a rate $1/T_c$ where T_c is the chip pulse duration. In the initial acquisition mode only, the period of $c(t)$ is assumed to be equal to the bit duration T for simplicity. The processing gain is given by $L = T/T_c$.

At time t, the observation vector received by the antenna array can be written as follows:

$$\begin{aligned} X(t) &= \psi(t)H(t) \otimes c(t)b(t) \\ &= \psi(t)\sum_{p=1}^{P} G_p(t)\varepsilon_p(t)b(t-\tau_p)c(t-\tau_p) + N(t) \end{aligned} \quad (1)$$

where $H(t) = \sum_{p=1}^{P} G_p(t)\varepsilon_p(t)\delta(t-\tau_p)$ is the channel response vector from the mobile to the antenna elements and $\otimes$ denotes time-convolution. $\tau_p \in [0, T)$ are the chip-asynchronous propagation time delays along the P paths, $p = 1, \ldots, P$ from the mobile to the antenna array, and $G_p(t)$ are the M-dimensional propagation vectors with equal norms, their value to be fixed later. For $m = 1, \ldots, M$, the mth component of $G_p(t)$ is the fading coefficient of the pth propagation path from the mobile to the mth antenna of the base station. These coefficients are Rayleigh distributed and further affected by the Doppler spread, path-loss, shadowing, and the power control transmit amplitude. $\varepsilon_p^2(t)$ represent the received power fractions along each path (i.e., $\sum_{p=1}^{P} \varepsilon_p^2(t) = 1$) of the total power $\psi^2(t)$ received from the desired user. The received power includes the normalization factor of the power fractions and hence it is also affected by path-loss, Rayleigh fading, and shadowing. The noise term $N(t)$ includes the thermal noise received at the antenna elements as well as the self-, in-cell, and out-cell interference.

A preprocessing unit in STAR (see Figs. 1 and 2) passes the above observation vector $X(t)$ through a matched-pulse filter[3] and provides the matched-filtering observation vector for frame number n over the time-interval $[0, 2T-T_c)$ in successive overlapping frames of period T by

$$Y_n(t) = \frac{1}{T_c}\int_{D_\phi} X(aT/2 + nT + t + t')\phi(t')\,dt' \quad (2)$$

[3]Please note that the model described is baseband without loss of generality. Both the carrier frequency modulation and demodulation steps can be embedded in the chip pulse-shaping and matched-filtering operations.

where D_ϕ denotes the temporal support[4] of the shaping pulse $\phi(t)$ and $a \in \{0, 1\}$ allows for a possible time shift by $T/2$ to avoid locating the frame edges in the middle of the delay spread [8]. For simplicity, we assume $a = 0$. After sampling at the chip rate and framing over $2L-1$ chip samples at the bit rate by the preprocessing unit (see Fig. 2), we obtain the $M \times (2L-1)$ matched-filtering observation matrix

$$\mathbf{Y}_n = [Y_n(0), Y_n(T_c), \ldots, Y_n((2L-2)T_c)]. \quad (3)$$

The structure of this matrix is detailed as follows:

$$\begin{aligned}\mathbf{Y}_n &= \sum_{k=-1}^{+1} \psi_n b_{n+k} \mathbf{Y}_{k,n} + \mathbf{N}_n \\ &= s_n \mathbf{Y}_{0,n} + \mathbf{I}_{\mathrm{ISI},n} + \mathbf{N}_n \simeq s_n \mathbf{Y}_{0,n} + \mathbf{N}_n \end{aligned} \quad (4)$$

where $s_n = \psi_n b_n = \psi(nT) b(nT)$ is the signal component, b_n is the transmitted DBPSK or DQPSK data sequence, and ψ_n^2 is the total received power. For $k = -1, 0, +1$, $\mathbf{Y}_{k,n}$ is the channel response $H(t)$ of (1), first convolved by the code segment that spreads b_{n+k}, then matched-filtered, sampled at the chip rate and buffered as follows:

$$\mathbf{Y}_{k,n} = [Y_{k,n}(0), Y_{k,n}(T_c), \ldots, Y_{k,n}((2L-2)T_c)] \quad (5)$$

$$Y_{k,n}(t) = \frac{1}{T_c} \int_{D_\phi} X_{k,n}(nT + t + t') \phi(t')\, dt' \quad (6)$$

$$X_{k,n}(t) = H(t) \otimes c(t) r(t - (n+k)T) \quad (7)$$

where $r(t)$ is a rectangular window with unit response over $[0, \mathrm{T})$. For simplicity, the system model of (4) does not identify explicitly the intersymbol interference (ISI) matrix $\mathbf{I}_{\mathrm{ISI},n}$ which represents the interference from adjacent symbols b_{n-1} and b_{n+1} but dumps it into the noise. $\mathbf{N}_n$, which results from the preprocessing of $N(t)$, is an uncorrelated additive noise vector due to thermal noise and to the other users in the system.

After despreading the matched-filtering observation matrix $\mathbf{Y}_n$ of (4) row-wise

$$Z_n(lT_c) = \frac{1}{L} \sum_{k=0}^{L-1} Y_n((l+k)T_c) c(nT + kT_c) \quad (8)$$

and framing the resulting post-correlation vector $Z(lT_c)$ over L chip samples at the bit rate

$$\mathbf{Z}_n = [Z_n(0), Z_n(T_c), \ldots, Z_n((L-1)T_c)] \quad (9)$$

we obtain the $M \times L$-dimensional post-correlation observation matrix $\mathbf{Z}_n$ of the post-correlation model (PCM) as follows [8]:

$$\mathbf{Z}_n = s_n \mathbf{H}_n + \mathbf{N}_{\mathrm{PCM},n} = b_n \psi_n \mathbf{G}_n \mathbf{\Upsilon}_n \mathbf{D}_n^T + \mathbf{N}_{\mathrm{PCM},n} \quad (10)$$

where $\mathbf{H}_n = \mathbf{G}_n \mathbf{\Upsilon}_n \mathbf{D}_n^T$ is the $M \times L$ spatio–temporal propagation matrix which yields $\mathbf{Y}_{0,n}$ after spreading $H(t)$ with the code segment of b_n, $\mathbf{G}_n = [G_{1,n}, \ldots, G_{P,n}] = [G_1(nT), \ldots, G_P(nT)]$ is the $M \times P$ spatial propagation matrix, and $\mathbf{\Upsilon}_n = \mathrm{diag}[\varepsilon_{1,n}, \ldots, \varepsilon_{P,n}] = \mathrm{diag}[\varepsilon_1(nT), \ldots, \varepsilon_P(nT)]$ is the $P \times P$ diagonal matrix of normalized power ratios over multipaths $\varepsilon_{p,n}^2$ (i.e., $\sum_{p=1}^{P} \varepsilon_{p,n}^2 = 1$). $\mathbf{D}_n = [D_{1,n}, \ldots, D_{P,n}]$ is the $L \times P$-dimensional time-response matrix with columns

$$D_{p,n} = [\rho_c(-\tau_{p,n}), \rho_c(T_c - \tau_{p,n}), \ldots, \rho_c((L-1)T_c - \tau_p)]^T$$

where $\{\tau_{p,n}\}_{p=1,\ldots,P} \in [0, T)$ are the time-varying multipath delays along the P paths and $\rho_c(t)$ is a truncated raised-cosine pulse which corresponds to the correlation function of a square-root raised-cosine shaping-pulse $\phi(t)$. Note that the equal norm of the vectors $G_{p,n}$ unspecified earlier is now fixed such that the norm of $\mathbf{H}_n$ is set to $\sqrt{M}$. $\mathbf{N}_{\mathrm{PCM},n}$ is the $M \times L$-dimensional spatio–temporal uncorrelated noise matrix after despreading with variance σ_N^2. It includes the thermal noise received at the antenna elements as well as the self-, in-cell, and out-cell interference. We define the input SNR after despreading as $SNR_{\mathrm{in}} = \psi^2/\sigma_N^2$ and assume the time variations of the channel to be very slow and locally constant relative to the bit duration T.

B. The 2-D-RAKE and the Early–Late Gate

The 2D-RAKE in [4]–[6] estimates the channel vector of a possible multipath at any chip sample as the principal eigenvector of the correlation matrix of the data vector despread at the corresponding chip sample. Let $\hat{R}_{ZZ,n}(k)$ denote the sample matrix obtained by simple smoothing of $Z_n(kT_c) Z_n(kT_c)^H$

$$\hat{R}_{ZZ,n}(k) = (1-\alpha)\hat{R}_{ZZ,n-1}(k) + \alpha Z_n(kT_c) Z_n(kT_c)^H \quad (11)$$

where $0 < \alpha \ll 1$ is a smoothing factor and $Z_n(kT_c)$ is the $(k+1)$th column of $\mathbf{Z}_n$. Let also $\hat{V}_n(k)$ and $\hat{\lambda}_n(k)$ denote the corresponding eigenvector[5] and eigenvalue estimates, respectively. The 2-D-RAKE selects the estimated multipath channel vectors and their time delays at the chips corresponding to the $P_{\max}$ maximum eigenvalues for $p = 1, \ldots, P_{\max}$ by

$$\hat{k}_{p,n} = \underset{k \in \{0,\ldots,L-1\} \setminus \{\hat{k}_{1,n},\ldots,\hat{k}_{p-1,n}\}}{\arg\max} \{\hat{\lambda}_n(k)\} \quad (12)$$

$$\hat{\tau}_{p,n} = \hat{k}_{p,n} T_c \quad (13)$$

$$\hat{G}_{p,n} = \hat{V}_n(\hat{k}_{p,n}). \quad (14)$$

This acquisition step is accurate only if the multipath delays are chip-synchronous (i.e., integer multiples of T_c) and constant in time. Due to its complexity, this procedure cannot be applied continuously during tracking.

To complete this initial acquisition step, we incorporate the early–late gate for tracking, a step not considered in [4]–[6]. For comparisons between the advanced and delayed data samples [2], [7], [11], [12], we replace the measurement of energy over one antenna in the conventional RAKE by a total energy measurement over all antennas.

First, assuming chip-oversampling at the rate $1/T_{sc} = k_s/T_c$, where $k_s > 1$ is an integer typically equal to 4, we compute the sample matrices $\hat{R}_{ZZ,n}^{+}(p)$ and $\hat{R}_{ZZ,n}^{-}(p)$ of $Z_{p,n}^{+} = Z_n(\hat{\tau}_{p,n} + T_{sc})$ and $Z_{p,n}^{-} = Z_n(\hat{\tau}_{p,n} - T_{sc})$,

[4]For a rectangular pulse, D_ϕ is $[0,\ T_c]$. In practice and as assumed in this paper, it is the temporal support of a truncated square-root raised-cosine.

[5]We assume that the norm of the eigenvectors is fixed to $\sqrt{M}$.

respectively, for each tracked path. Second, we extract the corresponding pair of eigenvector-eigenvalue estimates $\{\hat{V}_n^+(p), \hat{\lambda}_n^+(p)\}$ and $\{\hat{V}_n^-(p), \hat{\lambda}_n^-(p)\}$, respectively. Finally, we compare the energies of the advanced and delayed versions of the post-correlation vector around each tracked multipath, i.e., $\|Z_{p,n}^+\|^2$ and $\|Z_{p,n}^-\|^2$, for $p = 1, \ldots, P_{\max}$ [13]. The vector that has the higher energy represents the better update of the multipath time-delay and the corresponding propagation vector for the next iteration

$$a_{p,n} = \text{Sign}\{\|Z_{p,n}^+\|^2 - \|Z_{p,n}^-\|^2\} \tag{15}$$

$$\hat{\tau}_{p,n+1} = \hat{\tau}_{p,n} + a_{p,n} T_{sc} \tag{16}$$

$$\hat{G}_{p,n+1} = \begin{cases} \hat{V}_n^+(p), & \text{if } a_{p,n} = +1 \\ \hat{V}_n^-(p), & \text{if } a_{p,n} = -1. \end{cases} \tag{17}$$

In addition to the above contribution investigated in [13], we consider replacing the energy-based early–late decision rule of (15) by the following eigenvalue-based alternative rule [14]:

$$a_{p,n} = \text{Sign}\{\hat{\lambda}_n^+(p) - \hat{\lambda}_n^-(p)\} \tag{18}$$

which adds a "high-resolution" feature (i.e., based on signal subspace characterization) to the tracking step, well known for its increased robustness to noise. Indeed, the eigenvalues $\hat{\lambda}_n^+(p)$ and $\hat{\lambda}_n^-(p)$ are alternative measures of the signal energies in $\|Z_{p,n}^+\|^2$ and $\|Z_{p,n}^-\|^2$ in (15), and they significantly reduce the bias due to the noise in the observation energies $\|Z_{p,n}^+\|^2$ and $\|Z_{p,n}^-\|^2$.

To further improve the tracking performance and reduce timing errors, early–late loops may include an additional "clamped" state whereby the estimated time-delay is kept constant if the corresponding gap between the early–late measurements is below a given threshold. We incorporate this approach into the above eigenvalue-based loop as follows [14]:

$$a_{p,n} = \begin{cases} \text{Sign}\{\lambda_n^+(p) - \lambda_n^-(p)\}, \\ \qquad \text{if } |\lambda_n^+(p) - \lambda_n^-(p)| > \lambda_{\text{TH}} \\ 0, \quad \text{otherwise,} \end{cases} \tag{19}$$

$$\hat{\tau}_{p,n+1} = \hat{\tau}_{p,n} + a_{p,n} T_{sc} \tag{20}$$

$$\hat{G}_{p,n+1} = \begin{cases} \hat{V}_n^+(p), & \text{if } a_{p,n} = +1, \\ \hat{V}_n^-(p), & \text{if } a_{p,n} = -1, \\ \hat{V}_n^0(p), & \text{if } a_{p,n} = 0 \end{cases} \tag{21}$$

where λ_{TH} is the "clamping" threshold[6] over the gap between the early–late eigenvalues below which the time-delay estimate is not incremented. The new 2-D-RAKE early–late loop requires the additional computation of the sample matrix $\hat{R}_{ZZ,n}^0(p)$ of $Z_{p,n}^0 = Z_n(\hat{\tau}_{p,n})$ and its principal eigenvector $\hat{V}_n^0(p)$. Used later as a reference for performance comparisons, this enhanced version is found to offer up to 30% gain in capacity over that of (15)–(17) as previously suggested [13] for operation with the 2-D-RAKE.

[6]Note that the tracking response to fast time-delay drifts speeds up with larger thresholds while tracking errors decrease with smaller ones.

Neglecting the effect of synchronization errors, the despread vector-fingers $Z_{p,n} = Z_n(\hat{\tau}_{p,n})$ can be approximated at the estimated time-delays as

$$Z_{p,n} \simeq G_{p,n} s_{p,n} + N_{p,n} = G_{p,n} \psi_n \varepsilon_{p,n} b_n + N_{p,n}. \tag{22}$$

Due to the fact that the propagation vector estimates suffer from phase ambiguities, differential demodulation is required and implemented as follows for DBPSK:

$$\hat{s}_{p,n} = W_{p,n}^H Z_{p,n} = \hat{G}_{p,n}^H Z_{p,n}/M \tag{23}$$

$$\hat{s}_n = \text{Real}\left\{\sum_{p=1}^{P_{\max}} \hat{s}_{p,n} \hat{s}_{p,n-1}^*\right\} \tag{24}$$

$$\hat{b}_n = \text{Sign}\{\hat{s}_n\}. \tag{25}$$

For DQPSK, (24) and (25) are replaced by

$$\hat{s}_n = \sum_{p=1}^{P_{\max}} \hat{s}_{p,n} \hat{s}_{p,n-1}^* \tag{26}$$

$$\hat{b}_n = \text{Sign}\{\text{Real}[\hat{s}_n]\} + j\text{Sign}\{\text{Imag}[\hat{s}_n]\}. \tag{27}$$

In either case, the 2-D-RAKE thereby exploits the extra space diversity branches and the beamforming gain of the antennas in two consecutive space and time combining steps.

C. Overview of STAR

STAR replaces the two consecutive space and time-combining steps of the 2-D-RAKE by a joint operation in both space and time. It transforms the matrix $\mathbf{Z}_n$ into an ML-dimensional vector by arranging its columns in a single spatio–temporal column vector to obtain the following narrowband version of the PCM model [8] [see Fig. 1(a)]:

$$\underline{\mathrm{Z}}_n = \underline{\mathrm{H}}_n s_n + \underline{\mathrm{N}}_n \tag{28}$$

where $\underline{\mathrm{H}}_n$ and $\underline{\mathrm{N}}_n$, respectively, denote the vector-reshaped matrices $\mathbf{H}_n$ and $\mathbf{N}_n$ in (10). Using the above post-correlation vector, the channel identification unit of STAR provides a blind estimate (i.e., without a pilot) of the space–time channel vector $\underline{\hat{\mathrm{H}}}_n$ within a sign ambiguity for DBPSK or a quantized phase ambiguity (i.e., belongs to the QPSK constellation) for DQPSK [8]. It hence allows implementation of quasicoherent space–time MRC combining for DBPSK as follows [8]:

$$\hat{s}_n = \text{Real}\left\{\underline{\mathrm{W}}_n^H \underline{\mathrm{Z}}_n\right\} = \text{Real}\left\{\underline{\hat{\mathrm{H}}}_n^H \underline{\mathrm{Z}}_n/M\right\} \tag{29}$$

$$\hat{b}_n = \text{Sign}\{\hat{s}_n\}. \tag{30}$$

For DQPSK, quasicoherent MRC combining is implemented by

$$\hat{s}_n = \underline{\mathrm{W}}_n^H \underline{\mathrm{Z}}_n = \underline{\hat{\mathrm{H}}}_n^H \underline{\mathrm{Z}}_n/M \tag{31}$$

$$\hat{b}_n = \text{Sign}\{\text{Real}[\hat{s}_n]\} + j\text{Sign}\{\text{Imag}[\hat{s}_n]\}. \tag{32}$$

To resolve the quantized phase (sign for DBPSK) ambiguity of the channel estimate, the phase (sign for DBPSK) of $\hat{b}_n$ is differentially decoded as the information symbol estimate.

Multipath synchronization (i.e., both acquisition and tracking) is an implicit built-in step in the channel identification operation. It allows estimation of the number of multipaths $\hat{P}$, their time-delays $\hat{\tau}_{p,n}$ (i.e., $\hat{\mathbf{D}}_n$), relative powers $\hat{\varepsilon}^2_{p,n}$ (i.e., $\hat{\mathbf{\Upsilon}}_n$), and magnitudes and phases over all antennas in $\hat{\mathbf{G}}_n$. From these estimates, the channel identification unit reconstructs an accurate space–time channel vector estimate $\hat{\mathbf{H}}_n = \hat{\mathbf{G}}_n \hat{\mathbf{\Upsilon}}_n \hat{\mathbf{D}}_n^T$. A complete description of these operations is available in the original work on STAR [8]. Appropriate details will be given in the remainder of the paper when necessary.

The principal objective of this contribution is to assess the impact of synchronization on the improved 2-D-RAKE structure described earlier and STAR. The comparisons are carried out with an enhanced version of STAR that significantly reduces the complexity of the synchronization process while reducing its impact on performance.

III. Enhanced Synchronization in STAR

Below, enhancements of synchronization in terms of complexity and/or performance are introduced in both steps of multipath acquisition and tracking.

A. Improved Multipath Acquisition

1) Simplified Initial Multipath Detection: In the acquisition mode, the channel identification procedure of STAR, referred to as decision feedback identification (DFI) [8], converges to a rough estimate of the spatio–temporal propagation channel, denoted as $\hat{\mathbf{H}}_n$. From this estimate STAR forms a localization spectrum $\mathcal{S}_{\rm SS}(\tau)$ over all possible multipath delays $\tau \in [0, T)$; it then applies Root-MUSIC [15], a high-resolution localization technique, to detect the number of multipaths $\hat{P}$ and estimate their time-delays from the strongest peaks of the spectrum [8]. This localization approach is extremely accurate [i.e., 1/10 of a chip, see Fig. 3(a)], but computationally very expensive.

To reduce complexity significantly, we limit time-delay localization to a simple search over integer multiples of the chip duration. We arbitrarily fix the initial estimate of the number of multipaths $\hat{P}$ to $P_{\max}$ and identify the corresponding time-delay values as those of the $P_{\max}$ strongest values of $\mathcal{S}_{\rm SS}(kT_c)$ out of L, for $k = 0, \ldots, L-1$. The chip-sampled spectrum [see Fig. 3(b)] reduces to the following simple expression:

$$\mathcal{S}_{\rm SS}(kT_c) = \|\tilde{H}_{n,k}\|^2 \tag{33}$$

where $\tilde{H}_{n,k}$ is the kth column of $\tilde{\mathbf{H}}_n$ and allows a less accurate but still reliable initial time-delay estimation within a chip duration.

This simplified acquisition step allows the reconstruction of the space–time channel $\hat{\mathbf{H}}_n = \hat{\mathbf{G}}_n \hat{\mathbf{\Upsilon}}_n \hat{\mathbf{D}}_n^T$ (see above) as an initial estimate for permanent update by the tracking module. We thereby trade the high resolution localization of Root-MUSIC [15] in the acquisition step [8] for the high correction capabilities of the tracking module both in speed and accuracy.

2) Robust Multipath Detection Update: The tracking module of STAR repeatedly updates the identified number of multipaths unless otherwise instructed by a multipath detection update module. The detection module drops or adds a multipath

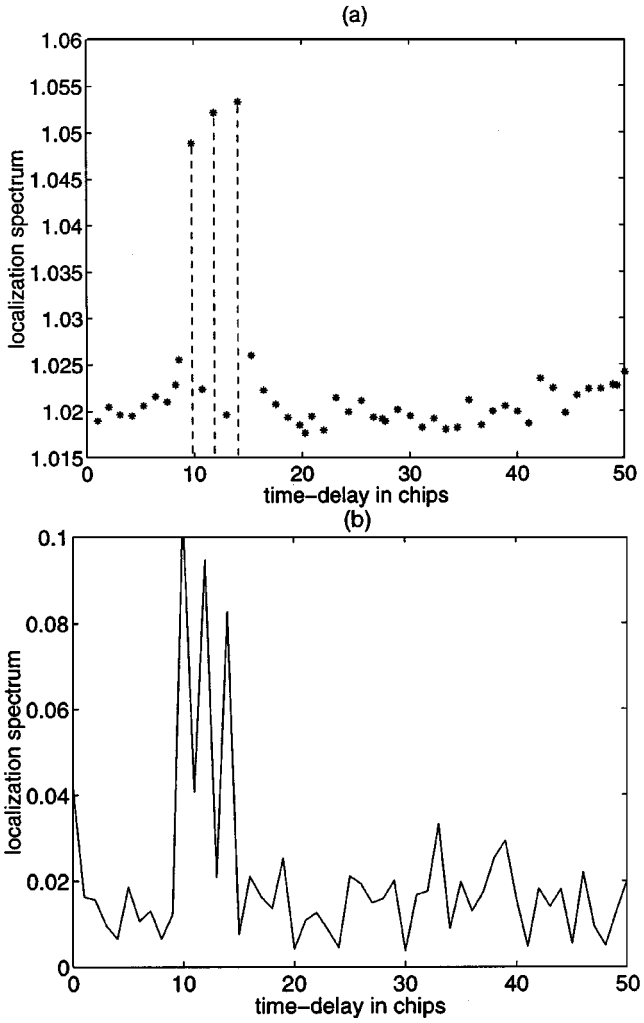

Fig. 3. (a) High resolution localization spectrum and its root solutions. (b) Simplified localization spectrum.

by comparing its energy to specified thresholds [8]. The robustness of the multipath detection update module becomes even more critical to tracking performance when we implement a simplified acquisition over a fixed number $P_{\max}$ of multipaths. Detection of excessive or missing paths should be quick and reliable to stabilize tracking and avoid drop/add cycles.

The multipath detection update rule in [8] has been set to compare energies of a vanishing or an appearing path against two critical thresholds $\varepsilon^2_{\min}$ and $\delta^2_{\max}$, respectively. Here, we explicitly link these thresholds to the residual noise estimate after coherent MRC combining, given for both DBPSK and DQPSK by

$$\hat{\sigma}^2_{\rm res} = (1-\alpha)\hat{\sigma}^2_{\rm res} + \alpha \left(\mathrm{Imag} \left\{ \hat{b}^*_n \underline{\hat{\mathrm{H}}}^H_n \underline{\mathrm{Z}}_n / M \right\} \right)^2 \tag{34}$$

where α is a smoothing factor. Additionally, we equate both thresholds $\varepsilon^2_{\min}$ and $\delta^2_{\max}$ to $\delta^2_{\rm TH}$ defined as

$$\delta^2_{\rm TH} = \kappa \frac{\hat{\sigma}^2_{\rm res}}{M} = \kappa \frac{\hat{\sigma}^2_N}{2M^2} \tag{35}$$

where $\hat{\sigma}^2_N = 2M\sigma^2_{\rm res}$ denotes an estimate of the input noise variance and κ a constant. With this new threshold, we introduce a minor update to the detection rule for a vanishing path but

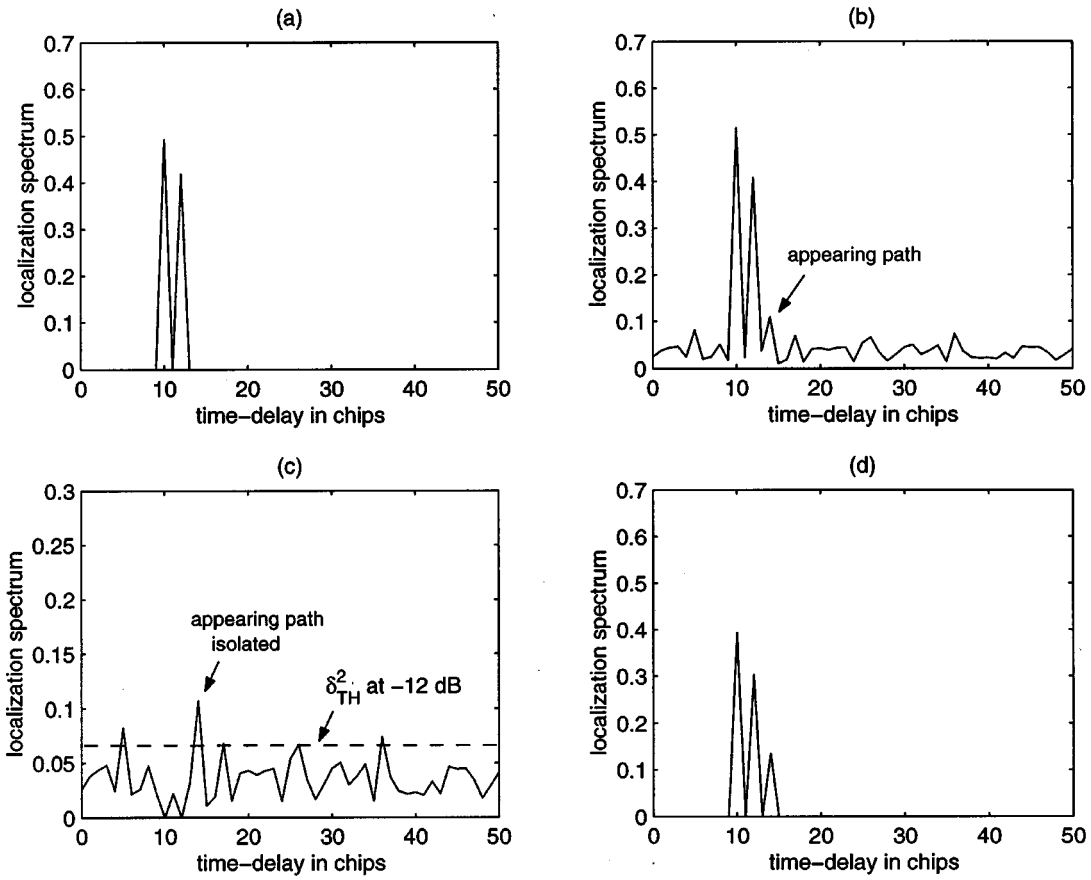

Fig. 4. Localization spectrum showing (a) the two paths being tracked using $\hat{\mathbf{H}}_n$, (b) the two paths being tracked along with the appearing one using $\breve{\mathbf{H}}_n$, (c) the power of the appearing path being constantly detected above the threshold δ^2_{TH} using the residual channel $\delta\hat{\mathbf{H}}_n$, and (d) the three paths being tracked using reconstructed $\hat{\mathbf{H}}_n$.

dramatically change the detection rule for an appearing path as explained below.

Vanishing Path: We decide that the pth path has vanished at block iteration n_d if then and for a number of previous block iterations $n_v - 1$ its power $\hat{\psi}^2_n\hat{\varepsilon}^2_{p,n}$ remains continuously below δ^2_{TH}, i.e.,

$$\hat{\psi}^2_n\hat{\varepsilon}^2_{p,n} < \delta^2_{\mathrm{TH}} \qquad \text{for } n \in \{n_d - n_v + 1, \ldots, n_d\}. \quad (36)$$

Appearing Path: The detection of an appearing path relies on a gross channel estimate $\breve{\mathbf{H}}_n$ provided by a DFI procedure almost identical to the one that estimates $\tilde{\mathbf{H}}_n$ in the acquisition step [8]. Like $\tilde{\mathbf{H}}_n$, $\breve{\mathbf{H}}_n$ is less accurate than $\hat{\mathbf{H}}_n$ because it does not reconstruct the channel from accurately tracked time-delay estimates. However, it incorporates all multipath components including those newly appearing.

We previously based the detection of an appearing path on the energy of the residual channel estimate $\delta\hat{\mathbf{H}}_n = \breve{\mathbf{H}}_n - \hat{\mathbf{H}}_n$ [8]. Here we propose a more robust estimation of the residual channel

$$\delta\hat{\mathbf{H}}_n = \breve{\mathbf{H}}_n\mathbf{\Pi}_{D_n} \quad (37)$$

where the $L \times L$ projector[7] $\mathbf{\Pi}_{D_n}$ is given by

$$\mathbf{\Pi}_{D_n} = \mathbf{I}_L - \hat{\mathbf{D}}_n\left(\hat{\mathbf{D}}_n^T\hat{\mathbf{D}}_n\right)^{-1}\hat{\mathbf{D}}_n^T \quad (38)$$

[7]Since $\hat{\mathbf{D}}_n^T\hat{\mathbf{D}}_n \simeq \mathbf{I}_{\hat{P}}$, inversion in (38) can be skipped.

and $\mathbf{I}_L$ is an $L \times L$ identity matrix. Additionally, we base detection on the chip-sampled residual spectrum defined as

$$\overline{\mathcal{S}}_{\mathrm{SS}}(kT_c) = \|\delta\hat{H}_{n,k}\|^2 \quad (39)$$

where $\delta\hat{H}_{n,k}$ is the kth column of $\delta\hat{\mathbf{H}}_n$.

At block iteration n_d, we avoid restarting acquisition [8] but decide that a new path has appeared at kth chip (i.e., $\hat{\tau}_{\hat{P}+1,n_d} = kT_c$) if, for a given number of block iterations n_a, $\overline{\mathcal{S}}_{\mathrm{SS}}(kT_c)$ continuously exceeds δ^2_{TH}, i.e.,

$$\overline{\mathcal{S}}_{\mathrm{SS}}(kT_c) > \delta^2_{\mathrm{TH}} \qquad \text{for } n \in \{n_d - n_a + 1, \ldots, n_d\}. \quad (40)$$

3) Illustration of the Detection Threshold: In Fig. 4, we illustrate the detection process of an appearing path. We select the 9.6-Kb/s voice-rate setup of Section IV-B with $M = 4$ antennas and operate at $SNR_{\mathrm{in}} \simeq -3$ dB after despreading. Fig. 4(a) shows that only two paths out of the three are being tracked while Fig. 4(b) shows that the third path previously dropped in a deep fade appears again. Fig. 4(c) shows that the residual spectrum detects a peak repeatedly exceeding δ^2_{TH} at about -12 dB for $n_a = 100$ consecutive symbols. Hence it readily instructs the tracking module to add the corresponding appearing path as shown in Fig. 4(d). Other noise bursts in Fig. 4(c) are ignored. They may exceed the threshold δ^2_{TH}, but only sporadically.

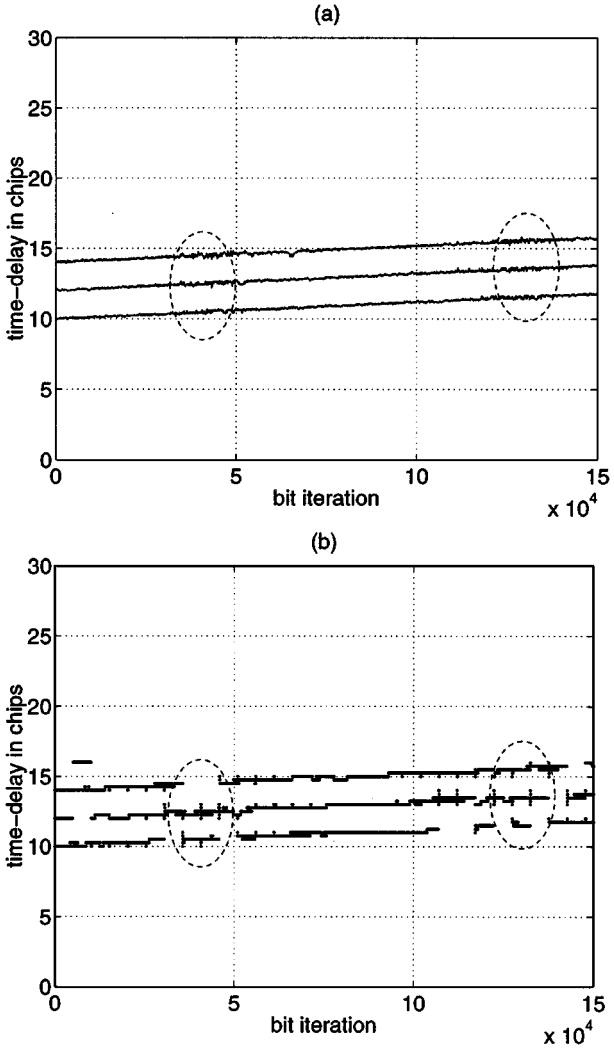

Fig. 5. Estimated time-delays $\hat{\tau}_{p,n}$ of (a) STAR and (b) 2-D-RAKE.

In general, with 1, 2, or 4 antennas, tuning of κ in (35) to achieve best robustness and stability of synchronization led to a low path detection threshold δ^2_{TH} ranging from -11 to -13 dB for enhanced STAR.[8] The original version of STAR does not rely on a detection threshold over multipath energy [8], hence a direct comparison is inappropriate. However, we have been able to measure the impact on performance of the suggested improvements in multipath detection update. They provide enhanced STAR with about a 20% gain in capacity over its original version in the three equal-power path situation[9] of Fig. 4.

Such improvements in multipath detection update actually increase the stability of the tracking process, which in turn translates into a capacity gain. Fig. 5(a) illustrates the high level of stability and accuracy achieved by enhanced STAR during the tracking process in the three equal-power path situation of Fig. 4. For comparison,[10] Fig. 5(b) illustrates the tracking performance of the new combination of the 2-D-RAKE with the eigenvalue-based early–late gate. It clearly shows more sensitivity, less stability, and lower accuracy in the highly adverse SNR situation under consideration. The two marked deep-fade regions in both Fig. 5(a) and (b) are of a particular interest. On one hand, Fig. 5(b) suggests that the 2-D-RAKE loses track of the useful paths and becomes relatively unstable. On the other hand, Fig. 5(a) indicates that STAR only sees a negligible increase in timing deviations while keeping solid track of the correct paths.[11]

Further investigation steps could have included useful performance measures specific to synchronization such as the probability of acquisition, probability of false alarm, mean time to lose lock, rms, timing jitter, etc. [12]. Rather, we orient the present work from a system-level point of view, a challenging step that ultimately measures the impact of synchronization directly on capacity and spectrum efficiency, the key figures for performance enhancement in wideband CDMA networks.

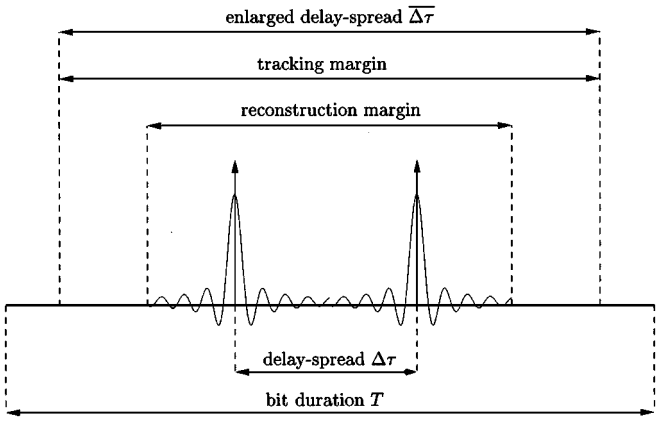

Fig. 6. Sizing and positioning of a reduced processing window around the delay spread inside the despread data frame of duration T.

B. Reduced Complexity of Multipath Tracking

1) Reduced Processing Window: STAR exploits the despread data available at all L chip samples in a frame duration T. However, channel measurements and characterizations in different urban and suburban environments indicate that typical values of the delay-spread rms are in the order of microseconds or nanoseconds for outdoor and indoor radio-channels, respectively (i.e., delay-spread of a few chips in 3G band) [16]. In relatively large processing gain situations, the desired signal is therefore confined to a shorter interval with length equal to the reconstruction margin in Fig. 6, which includes the truncated chip-pulse waveform around the delay-spread $\Delta\tau$. In this case, it is possible to lower the complexity of the tracking module significantly without loss in performance by limiting both signal extraction and channel identification to a reduced processing window inside the frame as in [10].

[8]Similar tuning of the new 2-D-RAKE and early–late gate combination led to a detection threshold of -9 dB.

[9]Other comparisons with relative power profiles of (0, -6, -10) dB or (0, -3, -6) dB led to similar observations.

[10]Original STAR [8] and the previous combination of the 2-D-RAKE with the energy-based early–late gate [13] both showed net degradation in tracking compared to their enhanced versions, respectively. Since the focus is not on these outdated versions, the corresponding plots were simply skipped.

[11]The snapshot of Fig. 4 was taken shortly after initial acquisition and right before fast stabilization of tracking.

If $\overline{\Delta\tau}$, illustrated in Fig. 6, denotes an arbitrarily enlarged delay-spread to allow an increased uncertainty margin (i.e., $\Delta\tau < \overline{\Delta\tau} < T$) for the tracking of time-varying multipaths due to clock drifts and receiver mobility, and if $L_{\overline{\Delta}} = \lceil \overline{\Delta\tau}/T_c \rceil$ is the corresponding length in chip samples, then we define the $M \times L_{\overline{\Delta}}$-dimensional reduced-size post-correlation matrix

$$\mathbf{Z}_n = [Z_n((L_0-1)T_c), \ldots, Z_n((L_0+L_{\overline{\Delta}}-1)T_c)] \quad (41)$$

where L_0 denotes an arbitrary chip offset which properly positions the reduced processing window around the delay spread. The dimensions of $\mathbf{H}_n$, $\mathbf{N}_n$, and $\mathbf{D}_n$ in (10) are thereby reduced to $M \times L_{\overline{\Delta}}$, $M \times L_{\overline{\Delta}}$, and $L_{\overline{\Delta}} \times P$, respectively, without further changes in the PCM structure. Hence, all STAR operations are carried out unchanged on $M \times L_{\overline{\Delta}}$-dimensional reduced-size data blocks with significant complexity savings in its tracking module.

2) Reduced Channel Identification Update Requirements: Channel identification is updated in STAR at the symbol-rate $R_s = 1/T$ [8], regardless of the coherence time T_{ch} over which the channel is considered as invariant [16]. Time-variations of the channel can be relatively slow, particularly in the high data-rate and low mobility situations. In this case, the channel identification update-rate can be reduced to a minimum of one symbol frame update out of $n_{\mathrm{ID}} \propto \lfloor R_s T_{ch} \rfloor$ with significant complexity savings in the tracking module of STAR. We update the DFI procedure of STAR [8] only at multiples $n' = \lfloor n/n_{\mathrm{ID}} \rfloor \times n_{\mathrm{ID}}$ of n_{ID} as follows:

$$\underline{\tilde{\mathrm{H}}}_{n'+n_{\mathrm{ID}}} = \underline{\hat{\mathrm{H}}}_{n'} + \mu \left(\underline{\mathrm{Z}}_{n'} - \underline{\hat{\mathrm{H}}}_{n'} \hat{s}_{n'} \right) \hat{s}^*_{n'} \quad (42)$$

then extract the enhanced channel estimate $\underline{\hat{\mathrm{H}}}_{n'+n_{\mathrm{ID}}}$ from $\underline{\tilde{\mathrm{H}}}_{n'+n_{\mathrm{ID}}}$ [8]. Otherwise, between two successive DFI updates, we keep the channel estimate constant by $\underline{\hat{\mathrm{H}}}_{n'+n''} = \underline{\hat{\mathrm{H}}}_{n'}$ for $n'' = 1, \ldots, n_{\mathrm{ID}} - 1$.

Note that during the above iterations only despreading and combining operations are active. One way to further reduce complexity dramatically is to freeze the very expensive despreading operation when keeping the channel estimate on hold [see Fig. 1(b)]. In this case, we carry out spatio–temporal combining over the matched-filtering observation matrix of (4) after $M(2L-1)\times$ one-dimensional vector reshaping as follows [17] [see Fig. 1(b)]:

$$\underline{\mathrm{Y}}_n \simeq s_n \underline{\mathrm{Y}}_{0,n} + \underline{\mathrm{N}}_n. \quad (43)$$

Hence, MRC combining operation for DBPSK in (29) is replaced by [14]:

$$\hat{s}_n = \mathrm{Real}\left\{ \underline{\mathrm{W}}_n^H \underline{\mathrm{Y}}_n \right\} = \mathrm{Real}\left\{ \frac{\underline{\hat{\mathrm{Y}}}_{0,n} \underline{\mathrm{Y}}_n}{\|\underline{\hat{\mathrm{Y}}}_{0,n}\|^2} \right\}. \quad (44)$$

For DQPSK, we replace (31) by the above equation without taking the real part.

Note that the reconstruction of $\underline{\hat{\mathrm{Y}}}_{0,n}$ for combining needs a respreading operation of $\underline{\hat{\mathrm{H}}}_n$ at each iteration when using long spreading codes. When using short codes, it becomes redundant after covering one code cycle and even unnecessary when the code period is equal to the symbol duration. Note also that the dimensions of both $\underline{\hat{\mathrm{Y}}}_{0,n}$ and $\underline{\mathrm{Y}}_n$ can be truncated to $M(L + L_{\overline{\Delta}} - 1) \times 1$ when using a reduced processing window.

As shown in the following subsection, the reduced channel update rate option reduces complexity significantly. However, it may degrade identification accuracy from relatively faster channel variations (i.e., n_{ID} times faster) and hence could result in severe performance losses. The resulting performance/complexity tradeoff will be discussed and illustrated by simulations in Section IV-D.

C. Complexity Assessment

The computational complexity order of both the 2-D-RAKE and STAR (with MRC before or after despreading, see above) is itemized in Table I along with the key processing operations they have in common, i.e., despreading, channel identification, MRC combining, tracking,[12] and reacquisition. Rough figures are provided in terms of average number of add–multiply operations needed per processed symbol.

In Table I, all despreading operations are implemented [14] using the OLA (overlap-add) FFT/IFFT-based fast convolution[13] technique [18], hence the complexity orders in $\log_2$. n_{CR} is the number of symbol iterations required before channel respreading and reconstruction of $\underline{\hat{\mathrm{Y}}}_{0,n}$ (see above). It is set to 1 for long codes and to n_{ID} for short codes with length L. n_{RA} denotes the 2-D-RAKE reacquisition period in symbol iterations while n_{SD} is the smoothing duration for sample matrix re-estimation.

For a better illustration of the table, we plot in Fig. 7 the complexity required per user in Mops for STAR and the 2-D-RAKE versus the processing gain L in 4.096 Mcps bandwidth with $M = 2$ antennas and $P_{\max} = P = 3$ multipaths. Complexity of the 2-D-RAKE takes into account multipath tracking by the early–late gate using (19)–(21) as well as multipath reacquisition over a smoothing duration of $n_{\mathrm{SD}} = 200$ symbols once every n_{RA} frames using (12)–(14).

Fig. 7(a) shows that the complexity of the 2-D-RAKE without reacquisition decreases slightly with lower data rates. The early–late gate may, however, lose lock over the multipaths, particularly at low SNR; hence periodic reacquisition is necessary to stabilize tracking. In this case, complexity increases with more frequent reacquisition, more so at lower data rates.

Fig. 7(b) shows that the complexity of the original version of STAR (i.e., full processing window and continuous channel update) increases fast at lower data rates. Even if it lies at a range closer from the 2-D-RAKE when the early–late gate and reacquisition are incorporated, it is still high. The proposed enhancements in synchronization reduce this complexity to an affordable order.

[12]The simulated 2-D-RAKE version implements the early–late gate with chip oversampling by a factor $k_s = 4$. For simplicity, the oversampling computational cost is not taken into account despite the resulting improvement in the 2-D-RAKE performance, leaving the possibility for early–late timing refinement with sampling clock shifts instead of chip oversampling.

[13]In [13], we implemented despreading with computationally more expensive time convolutions, hence the difference in complexity assessment there.

TABLE I
ESTIMATED COMPLEXITY ITEMS FOR BOTH THE 2-D-RAKE AND STAR (WITH MRC COMBING BEFORE/AFTER DESPREADING)

	2D-RAKE	STAR	
		MRC after Despreading	MRC before Despreading
Despreading	$MLP_{\max}$	$\{2L+4ML\}\log_2(2L_{\overline{\Delta}})$	$\frac{1}{n_{\rm ID}}\{2L+4ML\}\log_2(2L_{\overline{\Delta}})$
Channel ID	$\frac{1}{n_{\rm ID}}\{2M^2P_{\max}+M^3P_{\max}\}$	$\frac{1}{n_{\rm ID}}\{2ML_{\overline{\Delta}}\}$	$\frac{1}{n_{\rm ID}}\{2ML_{\overline{\Delta}}\}$
MRC	$MP_{\max}$	$ML_{\overline{\Delta}}$	$M\{L+L_{\overline{\Delta}}\}+\frac{1}{n_{\rm ID}}\{2PL_{\overline{\Delta}}\log_2(2L_{\overline{\Delta}})\}+\frac{1}{n_{\rm CR}}\{2ML\log_2(2L_{\overline{\Delta}})\}$
Tracking	$\frac{1}{n_{\rm ID}}\{2MLP_{\max}+2M^3P_{\max}+4M^2P_{\max}\}$	$\frac{1}{n_{\rm ID}}\{2PL_{\overline{\Delta}}\log_2(L_{\overline{\Delta}})\}$	$\frac{1}{n_{\rm ID}}\{2PL_{\overline{\Delta}}\log_2(L_{\overline{\Delta}})\}$
Reacquisition	$\frac{1}{n_{\rm RA}}(M^3L_{\overline{\Delta}})+\frac{n_{\rm SD}}{n_{\rm RA}}\{2M^2L_{\overline{\Delta}}+(2L+4ML)\log_2(2L_{\overline{\Delta}})\}$	negligible	negligible

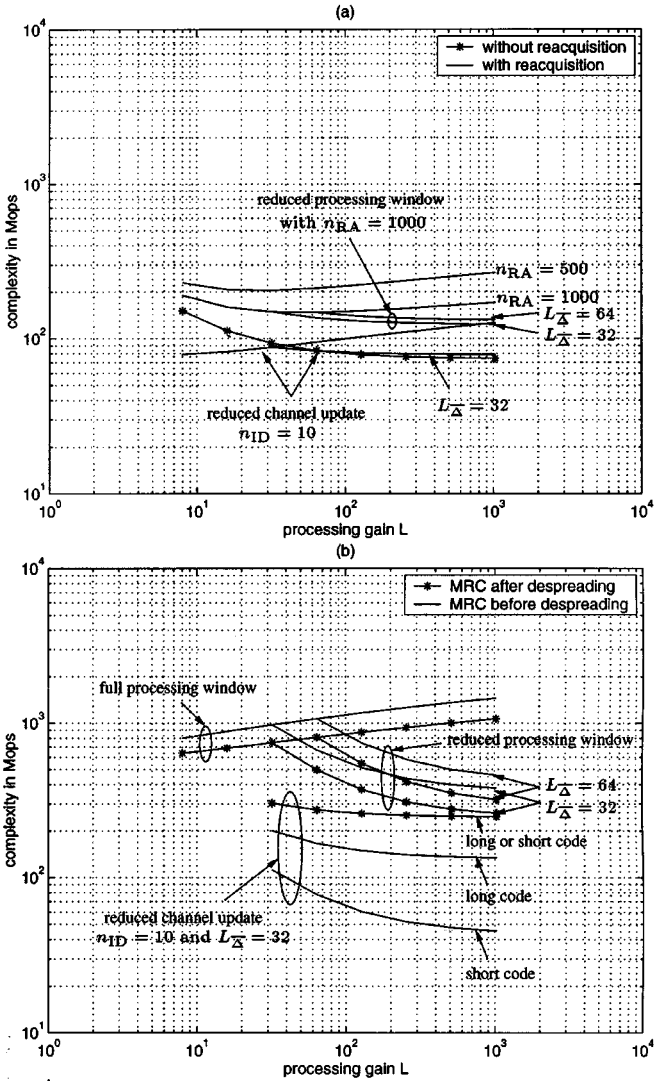

Fig. 7. Estimated complexity versus the processing gain L in 4.096 Mcps for $M=2$ antennas and $P=3$ multipaths. (a) 2-D-RAKE. (b) STAR.

Implementation of STAR over a reduced processing window, best suited to large processing gains, lowers complexity more dramatically at lower data rates. Whatever the size of the processing window, MRC after despreading is less complex than MRC before despreading with full channel update (no longer true with multiuser STAR [17]). Minimum channel identification update on the other hand, best suited to high data-rates, reduces complexity significantly for lower processing gains and favors implementation of MRC before despreading, more so when using a short code (see impact of code length on performance in [19]). The 2-D-RAKE similarly benefits from a reduced processing window and a minimum channel update in complexity reduction.

Overall, both complexity gains combined put STAR in the same computational order as the 2-D-RAKE (or even below, see Fig. 7). As one example, for a processing gain of 32 and $n_{\rm ID}=10$, STAR would require about 110 Mops with a short code and about 200 Mops with a long code against 90 Mops per user for the 2D-RAKE. Processors offer today a computational power of about 10 Gops and render STAR very attractive both in complexity and performance.

IV. SYSTEM-LEVEL ASSESSMENT AND SYNCHRONIZATION IMPACT

A. Uplink Capacity Evaluation Tool

We use the capacity computation tool based on the work in [20] for evaluation of both the 2-D-RAKE (or 1-D-RAKE when $M=1$) and STAR on the uplink. This tool populates a multicellular system with U spatially uniformly distributed mobiles up to the capacity of the cell with an outage probability fixed here to 1% and ensures that the received SNR meets the required value $SNR_{\rm req}$ for a given BER after channel decoding [20]

$$\text{Prob}\left(\sum_{u=1}^{U}\sum_{p=1}^{P} I_p^u g(\delta\tau_p^u) < \frac{L}{SNR_{\rm req}}\right) > 0.99 \qquad (45)$$

where I_p^u is the interference power from pth path of user number u, $\delta\tau_p^u \in [0,\, T_c)$ is the corresponding chip delay-mismatch relative to the sampling instants of the desired user, and $g(\delta\tau_p^u)$ is the energy of the shaping-pulse cross-correlation function $\rho_c(t)$.

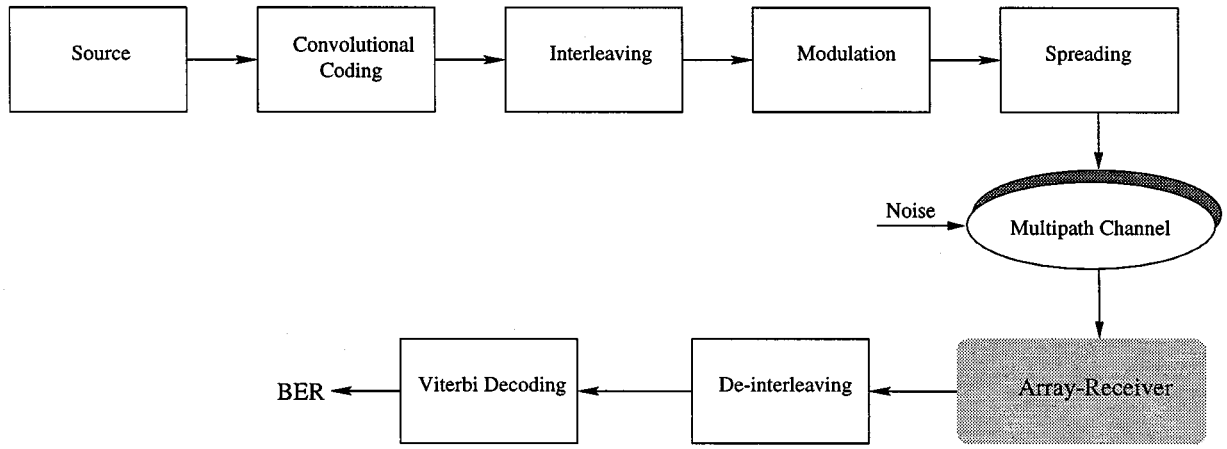

Fig. 8. Block diagram of link-level simulator.

In contrast to [20] and [21], where shaping pulses are square with duration T_c, we consider practical square-root raised cosine pulses truncated in such a way that the support of their cross-correlation function $\rho_c(t)$ is limited to $[-(N_c/2)T_c, (N_c/2)T_c]$. Hence we have (see curves on Fig. 9)

$$g(\delta\tau) \simeq \frac{1}{T_c^2} \sum_{k=-(N_c/2)}^{N_c/2} \rho_c^2(\delta\tau - kT_c) = \frac{1}{T_c^2} \sum_{k=-(N_c/2)}^{N_c/2} \left(\frac{\sin\{\pi(\delta\tau - k)\}}{\pi(\delta\tau - k)} \frac{\cos\{\pi\gamma(\delta\tau - k)\}}{1 - 4\gamma^2\pi(\delta\tau - k)^2} \right)^2 \tag{46}$$

where $\gamma \in [0, 1]$ denotes the rolloff factor.

The required SNR value SNR_{req} in (45) is actually found by binary search using the link-level simulator of Fig. 8. Most of the building blocks of this simulator were developed in [20]. Major modifications are, however, introduced in the array-receiver block to implement synchronization and combining with the 2-D-RAKE or STAR. The data signal generators were also modified to accommodate fast chip-level processing using an FFT/IFFT-based spreading block.

For a given noise level input σ_N^2, the link-level simulator processes a very large number of symbol frames and provides various statistics such as the average received power estimate $\hat{\psi}^2$ and the corresponding BER after channel decoding. The input noise level is hence adjusted by binary search until the required BER threshold is met, thereby determining the required SNR value $SNR_{\text{req}} = \hat{\psi}^2/\sigma_N^2$.

B. Simulation Setup

Unless specified otherwise, we use the following simulation setup parameters. We consider a wideband CDMA system with 5-MHz bandwidth and $P = 3$ equal-power paths. The mobile has a speed of 1 Kmph corresponding to a Doppler shift f_D of about 2 Hz at a carrier frequency of 2 GHz. The time-delays, initially set at $(10T_c, 12T_c, 14T_c)$, vary linearly in time, with a drift $d\tau/dt$ of 0.046 ppm. This drift is below the maximum clock imprecision thresholds of 0.05 and 0.1 ppm allowed by recent 3G standard proposals on the uplink and the downlink,

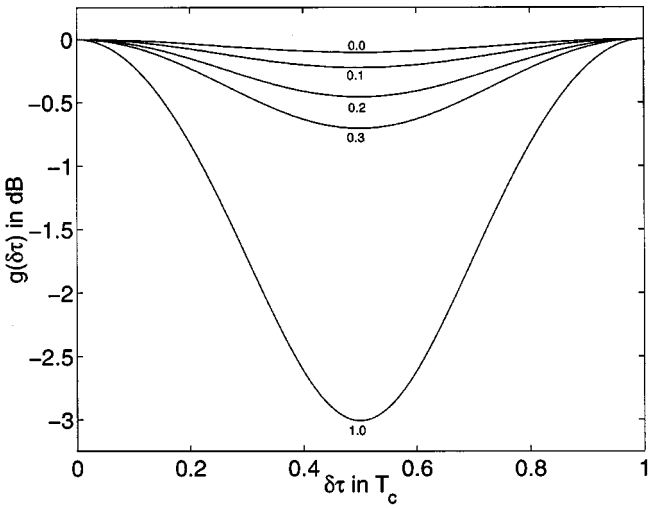

Fig. 9. Energy of chip-sampled raised cosine $g(\delta\tau)$ versus chip mismatch $\delta\tau$ for different rolloff factors.

respectively [22], [23]. The raised-cosine rolloff is fixed to 0 and the number of pulse samples is $N_c+1 = 17$ (i.e., truncated sinc). Power control (PC) requests an incremental change of ± 0.25 dB in transmitted power every 0.625 ms with a delay of 0.625 ms and an error of 10% over the PC bit command. The user information is encoded using a rate 1/2 convolutional code with constraint length $K = 9$. We consider a DBPSK voice rate of 9.6 Kb/s with processing gain $L = 256$ and a DQPSK high data-rate of 128 Kb/s with processing gain $L = 32$.

We estimate the uplink capacities by simulations using the parameters $k_s = 4$, $n_{\text{SD}} = 200$, and $n_{\text{RA}} = 1000$ for the 2-D-RAKE, and with $L_{\overline{\Delta}} = 32$ and $n_{\text{ID}} = 1$ for both the 2D-RAKE and STAR.[14] The target BER is fixed here to 10^{-3} and 10^{-5} for the 9.6 and 128 Kb/s data-rates, respectively. Simulations are run in parallel with perfect and active synchronization. They provide results in terms of SNR_{req}, capacity C in number of users per cell, and spectrum efficiency in b/s/Hz/antenna defined as $\zeta = p_{\text{Tx}}C/[(2ML) \times (1+\gamma)]$ for DBPSK and as $\zeta = p_{\text{Tx}}C/[(ML) \times (1+\gamma)]$ for DQPSK, where the factor $(1+\gamma)$

[14]Compared to their full processing window versions, the 2-D-RAKE and STAR with a reduced processing window showed no degradation in performance for both data-rates.

takes into account the rolloff excess bandwidth.[15] The activity factor p_{Tx} is fixed to 45% and 100% for the voice and data[16] rates, respectively.

C. Antenna-Array Dimension

In a first set of simulations, we measure the impact of timing errors on the uplink performance of the 2-D-RAKE and STAR array-receivers with the number of antennas taking the values $M = 1, 2,$ and 4.

Performance results for the 9.6 Kb/s voice-rate in Table II suggest the following.

- With the 2-D-RAKE, we measure a loss of about 1.1 dB in required SNR and 25% in capacity or spectrum efficiency due to the sole effect of timing errors when $M = 4$. Degradation of STAR is only of 0.7 dB for SNR loss and 15% for capacity or spectrum efficiency, showing greater robustness to timing errors and a better exploitation of antenna arrays. Capacity or spectrum efficiency increases with more antennas. The relative gain decreases, however, due to increased synchronization errors at the lower operating SNR values.
- STAR increases its performance advantage in spectrum efficiency per antenna over the 2-D-RAKE from about 50% to 60% with perfect synchronization (i.e., advantages derived from channel identification and combining) to around 70% to 100% in the presence of timing errors (i.e., additional advantage due to enhancement of synchronization). The highest relative gain is achieved with one antenna where STAR outperforms the 1-D-RAKE by about 100% in spectrum efficiency.

Performance results for the 128 Kb/s data-rate in Table III suggest the following.

- As expected for high data-rates, lower capacity values are noted. The capacity being almost inversely proportional to SNR, relatively larger changes in SNR are required to achieve noticeable changes in capacity since the number of supported mobiles is much smaller. Hence, SNR losses due to timing errors impact capacity differently for high data-rates, although figures are roughly the same as in the 9.6 Kb/s case for either receiver.
- Capacity figures for the 2-D-RAKE and STAR are closer when synchronization is perfect. However, losses in capacity or spectrum efficiency due to timing errors are much higher for the 2-D-RAKE when compared to STAR. Overall, STAR increases spectrum efficiency by about 100% and 80% with 2 or 4 antennas, respectively.
- With a single antenna the 128-Kb/s data-rate is not achievable, neither by the 1-D-RAKE nor by STAR (despite SNR gains). Antenna arrays of at least two elements are required in order to accommodate this high-data rate in a wideband CDMA network.

In the following, we work with an antenna-array of four elements, a configuration smaller in dimension than the common setup of six antennas per cell-site (with three sectors and two antennas per sector).

TABLE II
IMPACT OF SYNCHRONIZATION ON PERFORMANCE OF BOTH THE 2-D-RAKE AND STAR AT 9.6 Kb/s

	9.6 Kb/s (DBPSK) @ 10^{-3}			
	2D-RAKE		STAR	
	Ideal Sync.	Active Sync.	Ideal Sync.	Active Sync.
	$M = 1$ antenna			
SNR_{req} (dB)	3.9	4.7	2.1	2.3
C (users/cell)	71	53	112	108
ζ (bps/Hz/antenna)	0.062	0.047	0.098	0.095
	$M = 2$ antennas			
SNR_{req} (dB)	1.1	1.8	-0.7	-0.3
C (users/cell)	172	137	269	247
ζ (bps/Hz/antenna)	0.076	0.060	0.12	0.11
	$M = 4$ antennas			
SNR_{req} (dB)	-1.8	-0.7	-3.4	-2.7
C (users/cell)	357	276	533	456
ζ (bps/Hz/antenna)	0.078	0.060	0.12	0.10

TABLE III
IMPACT OF SYNCHRONIZATION ON PERFORMANCE OF BOTH THE 2-D-RAKE AND STAR AT 128 Kb/s

	128 Kb/s (DQPSK) @ 10^{-5}			
	2D-RAKE		STAR	
	Ideal Sync.	Active Sync.	Ideal Sync.	Active Sync.
	$M = 1$ antenna			
SNR_{req} (dB)	8.3	9.1	7.2	7.4
C (users/cell)	0	0	0	0
ζ (bps/Hz/antenna)	0	0	0	0
	$M = 2$ antennas			
SNR_{req} (dB)	4.8	6.0	4.3	4.4
C (users/cell)	2	1	3	2
ζ (bps/Hz/antenna)	0.031	0.016	0.047	0.031
	$M = 4$ antennas			
SNR_{req} (dB)	1.9	2.9	1.3	1.6
C (users/cell)	6	4	8	7
ζ (bps/Hz/antenna)	0.047	0.031	0.063	0.055

D. Fast Channel Case

In a second set of simulations, we measure the impact of synchronization on the 2-D-RAKE and STAR in the presence of

[15]The additional excess bandwidth due to pulse truncation is not taken into account for simplicity.

[16]Note that expected values for ζ at 10^{-5} should be weaker.

fast channel parameter variations [14]. We increase the Doppler shift f_D to about 106 Hz and increase the delay drift $d\tau/dt$ up to 4 ppm, far beyond the 0.05 and 0.1 ppm uplink/downlink clock imprecision thresholds mentioned above. Performance results shown in Table IV suggest the following.

- Timing impact may become negligible in the presence of high Doppler even in the presence of very fast time-delay drifts. In this situation, channel identification errors stand out as the dominant factor in performance degradation compared to the sole effect of timing errors, more so at lower data rates. In the voice-rate case, the 2-D-RAKE and STAR with perfect timing incur about 50% and 20% loss in spectrum efficiency, respectively, due to the Doppler increase by a factor 50 (see perfect timing results in Table II). Activation of timing with a delay drift 90 times faster adds just about 10% and 20% loss, respectively. In the high-rate case where channel variations are relatively slower, the additional impact of timing errors become far more significant, more so with the 2-D-RAKE. Activation of synchronization incurs almost 50% and 20% loss in spectrum efficiency to the 2-D-RAKE and STAR, respectively.
- Overall, the performance advantage noted for STAR over the 2-D-RAKE increases in the presence of faster channel parameter variations. We measure spectrum efficiency gains of about 110% and 100% for the voice and data rates, respectively, against the approximate 70% and 80% gains reported previously in the case of slow channel parameter variations (see Tables II and III).

As discussed earlier in Sections III-B-1 and III-B-2, reduced channel update also increases channel parameter variations and translates into performance losses. However, it reduces complexity significantly. We summarize below the resulting tradeoff between the complexity gain and the spectrum efficiency loss for both cases of slow and fast channel parameter variations using $n_{\mathrm{ID}} = 10$.

With the channel update rate reduced by a factor 10, the 2-D-RAKE and STAR gain about 40% and 55% in complexity in the voice-rate case and about 40% and 75% in the data-rate case, respectively (see Fig. 7). However, both the Doppler and the multipath delay-drifts become ten times faster, relatively. In the slow channel case, increased channel variations from reduced update are not fast enough yet to result in noticeable degradation in performance. We measure no loss in spectrum efficiency for both data rates. The reduced channel update option is extremely useful in this case.

In the fast channel case, however, the 2-D-RAKE and STAR incur 50% and 25% loss in spectrum efficiency in the data-rate case, at 0.008 and 0.023 b/s/Hz/antenna, respectively. At the voice-rate, channel variations become relatively fast and performance losses become unacceptable for both the 2-D-RAKE and STAR. The reduced channel update option may still be useful in the high data-rate case of most interest to future wideband CDMA networks. However, if trading 25% performance loss for 75% complexity reduction is acceptable with STAR, trading 50% performance loss for 40% complexity reduction is not acceptable with the 2-D-RAKE. Even then STAR with $n_{\mathrm{ID}} = 10$ will outperform the 2-D-RAKE with $n_{\mathrm{ID}} = 1$ by about 50% in spectrum efficiency while requiring almost the same complexity cost.

TABLE IV
IMPACT OF SYNCHRONIZATION ON PERFORMANCE OF BOTH THE 2-D-RAKE AND STAR AT FAST DOPPLER AND MULTIPATH DELAY-DRIFTS

	f_D = 106 Hz, $\frac{d\tau}{dt}$=4 ppm			
	2D-RAKE		STAR	
	Ideal Sync.	Active Sync.	Ideal Sync.	Active Sync.
	9.6 Kb/s (DBPSK) @ 10^{-3}			
SNR_{req} (dB)	1.1	1.5	-2.3	-1.6
C (users/cell)	179	163	424	348
ζ (bps/Hz/antenna)	0.039	0.036	0.093	0.077
	128 Kb/s (DQPSK) @ 10^{-5}			
SNR_{req} (dB)	2.8	6.1	2.1	2.3
C (users/cell)	4	2	5	4
ζ (bps/Hz/antenna)	0.031	0.016	0.039	0.031

E. Impact of Chip-Pulse Distortion

Simulation results above demonstrate that STAR outperforms the 2-D-RAKE in spectrum efficiency due to enhancements in both combining and synchronization. Improvement in combining can be attributed to the fact that the quasicoherent demodulation and differential decoding in STAR perform better than the differential demodulation of the 2-D-RAKE. On the other hand, the enhancement in synchronization suggests a new interpretation, that the pulse matching approach of STAR is superior in performance to the finger extraction principle of the 2-D-RAKE.

One concern that arises in this case is whether STAR is more sensitive to waveform distortions than the 2-D-RAKE since it matches the nominal chip-pulse waveform, an essential assumption to the tracking and combining steps in STAR. The answer will determine whether STAR could maintain its performance advantage over the 2-D-RAKE in more practical operating conditions. Standard proposals indeed tolerate an amount of waveform distortions [22], [23]. In a third set of simulations, we assess the impact of chip-pulse distortions over capacity and spectrum efficiency [14].

We define[17] the pulse distortion in percentage points as the square root of the energy of the pulse waveform error over the energy of the pulse waveform itself. For a given distortion ratio, we generate $N_c + 1$ i.i.d. random Gaussian noise samples with the appropriate energy and add them to the nominal pulse waveform samples in the received signals. Errors are independent from one symbol to another.

In Fig. 10, we plot the capacity and spectrum efficiency performance in the voice-rate case for both the 2-D-RAKE and STAR versus the pulse distortion amount in %. Curves suggest the following.

[17]This definition is similar to that suggested by recent 3G standard proposals [22], [23].

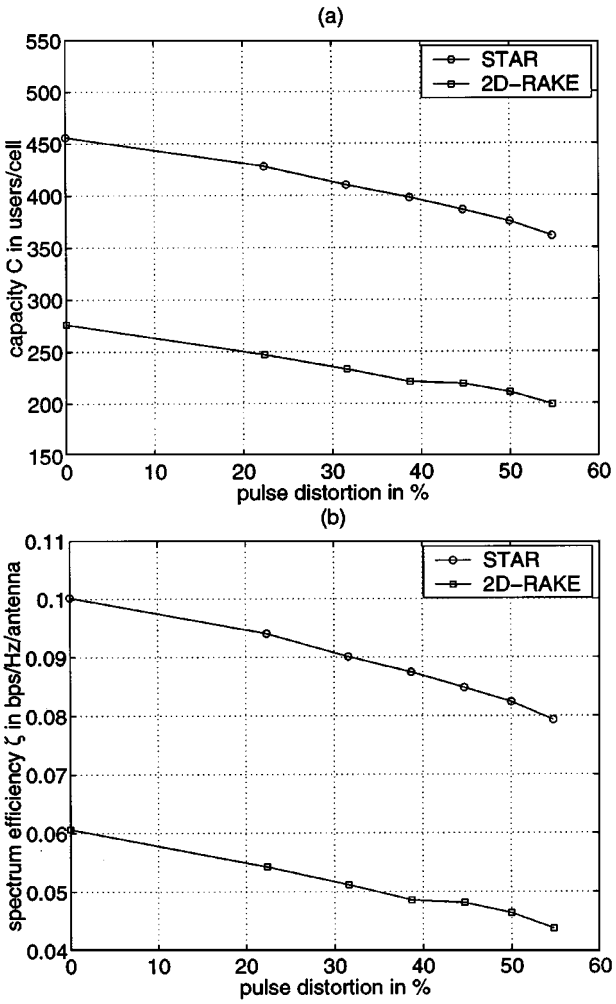

Fig. 10. Impact of pulse distortion on (a) capacity and (b) spectrum efficiency at 9.6 Kb/s.

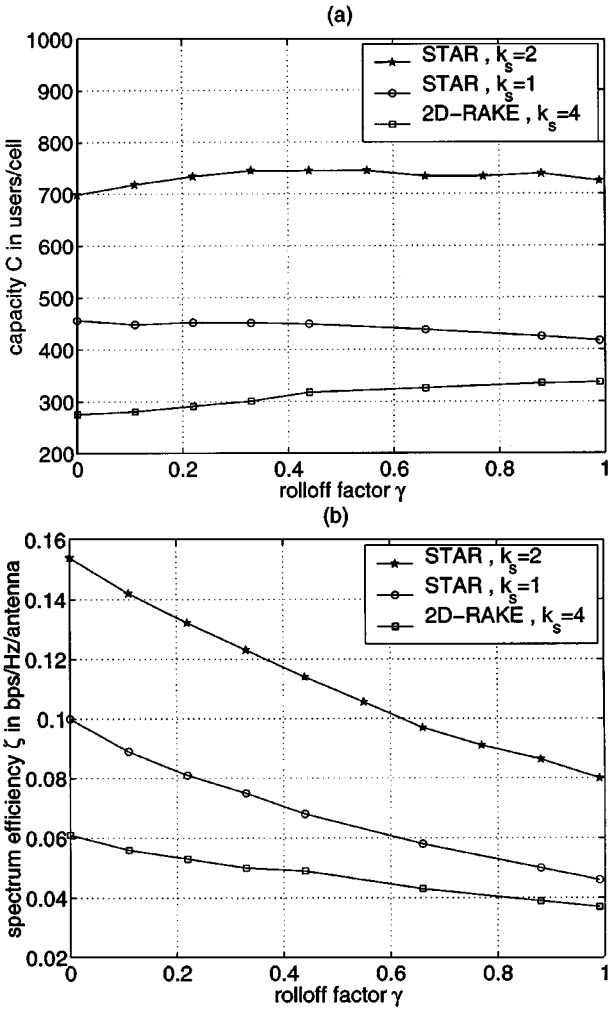

Fig. 11. Impact of rolloff factor γ on (a) capacity and (b) spectrum efficiency at 9.6 Kb/s.

- Capacity and *a fortiori* spectrum efficiency decrease almost linearly with the distortion energy, a signal leakage processed as interference to the receiver.
- Standards suggest maximum distortion thresholds of 12.5% and 17.5% on the uplink and downlink, respectively. Performance degradation due to a pulse distortion of 15% is modest, less than 5% for both the 2-D-RAKE and STAR.
- Even though STAR matches the nominal waveform while the 2-D-RAKE extracts fingers (i.e., pulse peaks), pulse distortions impact the performance of both receivers in the same way. This suggests that STAR maintains its performance advantage over the 2-D-RAKE due to enhanced synchronization even in the presence of pulse waveform distortions.

F. Impact of Rolloff Selection and Oversampling

Another concern that may question the established performance advantage of STAR over the 2-D-RAKE is the rolloff factor selection. For illustration purposes and for simplicity, timing gains have been demonstrated with a sinc function (i.e., rolloff 0). For practical design purposes though, systems would implement raised-cosine filters with a rolloff factor higher than 0 to avoid sharp spectral decays. Standard proposals suggest a rolloff factor of 0.22 [22], [23]. STAR would then extract and match pulses sampled at a rate lower than their bandwidth.

The question that arises in this case is whether STAR would lose its performance advantage over the 2-D-RAKE due to possible timing degradation from a sampling rate below the bandwidth. In a fourth set of simulations, we hence assess the impact of rolloff factor selection on performance (assuming a bandwidth higher than 5 MHz) [14]. Capacity and spectrum efficiency results shown in Fig. 11 versus the rolloff factor in the voice-rate case suggest the following.

- As anticipated in [8], STAR without chip oversampling is extremely robust to the pulse waveform design (see [24], [25] for specific work on waveform design and selection). By linear phase fitting in the frequency domain, it always extracts from the received chip waveform the closest sinc pulse in the tracking process [8]. It hence delivers about the same capacity performance even if the raised-cosine shaping pulse occupies a bandwidth higher than the chip-rate. Degradation due to frequency aliasing becomes noticeable only at rolloff factors close to 1, but it remains negligible.

- The 2-D-RAKE, with an oversampling factor $k_s = 4$, reduces its sensitivity to timing errors and slightly increases its capacity performance at higher rolloff factors. Yet at a rolloff factor of 0.22 [22], [23], STAR advantage over the 2-D-RAKE is still significant at about 55% in spectrum efficiency.
- In light of the above observations, we investigated the impact of chip oversampling on STAR by a factor $k_s = 2$. Oversampling virtually doubles the processing gain with practically no increase in computational order (see Fig. 7), yet it introduces a "sampling diversity" gain that further underlines the strength of the pulse-matching approach of STAR versus finger extraction in RAKE-type receivers. Indeed, STAR capacity enhancement due to oversampling is very significant and increases from about 55% for $\gamma = 0$ to about 75% for $\gamma = 1$. The capacity increase at higher rolloffs indicates that oversampling above the chip-rate avoids aliasing (see above) as already shown in fractional sampling in equalization [3] and enables exploitation of increasing robustness to timing errors. At a rolloff of 0.22 [22], [23], the spectrum efficiency advantage of STAR with oversampling by factor 2 over the 2D-RAKE with oversampling by factor 4 is very high at about 150%.

Overall, it is worth noting that STAR avoids chip oversampling and that its resolution is not limited by a fixed refining chip-fraction. It exploits the signal energy from the entire shaping pulse, not only its peak (i.e., RAKE-finger), hence it generates better estimates for the delay of each path despite possible waveform distortions. It identifies a stronger space–time channel vector instead of separate multipath channel vectors with weaker fractioned powers. Without a pilot, it achieves coherent detection and differential decoding instead of less efficient differential demodulation. Overall, STAR outperforms both the 2-D-RAKE in space–time signal combining and the early–late gate in synchronization. At practically the same order of complexity, performance gains are significant with one (i.e., 1-D-RAKE) or more antennas, for low or high data rates, for slow or fast channel variations.

V. Conclusion

Synchronization errors with the early–late gate may have a serious impact on performance of wideband CDMA networks. They may cancel improvement in SNR or capacity achieved at other system levels. The 2-D-RAKE with the early–late gate is more sensitive to synchronization errors than STAR: the performance gain of STAR over the 2-D-RAKE with perfect timing increases when synchronization is activated and may reach up to 100% in spectrum efficiency with one (i.e., 1-D-RAKE) or more antennas at both 9.6- and 128-Kb/s data-rates. This gain further increases in high Doppler and fast multipath delay-drifts. Data oversampling above the chip-rate favors STAR even more. These advantages, proved valid even in the presence of pulse-waveform distortions, demonstrate the superiority of the chip-pulse matching approach of STAR over the finger extraction principle of the RAKE-type receivers. Significant enhancements to synchronization in terms of computational costs and multipath detection resolution and stability have been proposed, which render STAR an affordable receiver solution and hence very attractive both in performance and complexity for wideband CDMA networks.

Acknowledgment

The authors would like to thank A. Jard, H. El-Nahas, and W. Navarro of Nortel Networks, Paris, for fruitful discussions about several issues treated in this paper as well as J. Dugan of Nortel Networks, Ottawa, for cross-validating parts of the complexity assessments.

References

[1] R. Prasad and T. Ojanperä, "An overview of CDMA evolution toward wideband CDMA," *IEEE Commun. Surveys*, vol. 1, Fourth Quarter 1998.

[2] A. Viterbi, *CDMA Principles of Spread Spectrum Communication*. New York: Addison-Wesley, 1995.

[3] J. K. Tugnait, L. Tong, and Z. Ding, "Signal-user channel estimation and equalization," *IEEE Signal Processing Mag.*, vol. 17, pp. 17–28, May 2000.

[4] B. Suard, A. Naguib, G. Xu, and A. Paulraj, "Performance analysis of CDMA mobile communication systems using antenna arrays," in *Proc. ICASSP'93*, vol. VI, 1996, pp. 2421–2424.

[5] B. H. Khalaj, A. Paulraj, and T. Kailath, "2D RAKE receivers for CDMA cellular systems," in *Proc. GLOBECOM'94*, 1994, pp. 400–404.

[6] A. F. Naguib, "Adaptive antennas for CDMA wireless networks," Ph.D. dissertation, Stanford Univ., Stanford, CA, 1996.

[7] R. De Gaudenzi, M. Luise, and R. Viola, "A digital chip timing recovery loop for band-limited direct-sequence spread-spectrum signals," *IEEE Trans. Commun.*, vol. 41, pp. 1760–1769, Nov. 1993.

[8] S. Affes and P. Mermelstein, "A new receiver structure for asynchronous CDMA: STAR—The spatio–temporal array-receiver," *IEEE J. Select. Areas Commun.*, vol. 16, pp. 1411–1422, Oct. 1998.

[9] S. Affes, A. Louzi, N. Kandil, and P. Mermelstein, "A high capacity CDMA array-receiver requiring reduced pilot power," in *Proc. GLOBECOM'2000*, vol. 2, 2000, pp. 912–916.

[10] M. D. Zoltowski and J. Ramos, "Blind multi-user access interference cancellation for CDMA based PCS/cellular using antenna arrays," in *Proc. ICASSP'96*, vol. 5, 1996, pp. 2730–2733.

[11] W. Sheen and G. L. Stüber, "Effects of multipath fading on delay-locked loops for spread spectrum systems," *IEEE Trans. Commun.*, vol. 42, pp. 1947–1956, Feb./Mar./Apr. 1994.

[12] M. K. Simon, J. Omura, R. A. Scholtz, and B. K. Levitt, *Spread Spectrum Communications*. Rockville, MD: Computer Science Press, 1985, vol. I–III.

[13] K. Cheikhrouhou, S. Affes, and P. Mermelstein, "Impact of synchronization on receiver performance in wideband CDMA networks," in *Proc. 34th Asilomar Conf. Signals, Systems, and Computers*, 2000, pp. 252–258.

[14] ——, "Synchronization sensitivity of enhanced CDMA array-receivers to fast channel time-variations and to shaping-pulse design," in *Proc. 35th Asilomar Conference on Signals, Systems, and Computers*, Pacific Grove, Nov. 4–7, 2001, to be published.

[15] A. J. Barabell, "Improving the resolution performance of eigenstructure-based direction-finding algorithms," in *Proc. ICASSP'83*, vol. 1, 1983, pp. 336–339.

[16] T. S. Rappaport, *Wireless Communications, Principles and Practice*. Englewood Cliffs, NJ: Prentice Hall, 1996.

[17] S. Affes, H. Hansen, and P. Mermelstein, "Interference subspace rejection in wideband CDMA—Modes for mixed-power operation," in *Proc. ICC'01*, vol. 2, 2001, pp. 523–529.

[18] J. J. Shynk, "Frequency-domain and multirate adaptive filtering," *IEEE Signal Processing Mag.*, vol. 9, pp. 14–37, Jan. 1992.

[19] S. Parkvall, "Variability of user performance in cellular DS-CDMA—Long versus short spreading sequences," *IEEE Trans. Commun.*, vol. 48, pp. 1178–1187, July 2000.

[20] A. Jalali and P. Mermelstein, "Effects of diversity, power control, and bandwidth on the capacity of microcellular CDMA systems," *IEEE J. Select. Areas Commun.*, vol. 12, pp. 952–961, June 1994.
[21] D. J. Torrieri, "Performance of direct-sequence systems with long pseudonoise sequences," *IEEE J. Select. Areas Commun.*, vol. 10, pp. 770–781, May 1992.
[22] 3rd Generation Partnership Project (3GPP), Technical Specification Group (TSG), Radio Access Network (RAN), and Working Group (WG4), "UE radio transmission and reception (FDD),", TS 25.101, V3.4.1, 2000.
[23] ——, "Base station conformance testing (FDD),", TS 25.141, V3.3.0, 2000.
[24] T. F. Wong, T. M. Lok, and J. S. Lehnert, "Asynchronous multiple-access interference suppression and chip waveform selection with *aperiodic* random sequences," *IEEE Trans. Commun.*, vol. 47, pp. 103–114, Jan. 1999.
[25] M. A. Landolsi and W. E. Stark, "DS-CDMA chip waveform design for minimal interference under bandwidth, phase, and envelope constraints," *IEEE Trans. Commun.*, vol. 47, pp. 1737–1746, Nov. 1999.

Karim Cheikhrouhou received the Diplôme d'Ingénieur and M.Sc. degrees in telecommunications from the École Supérieure des Communications de Tunis, Tunisia, and the École Nationale d'Ingénieurs de Tunis, Tunisia, in 1993 and 1996, respectively. He is currently pursuing the Ph.D. degree in telecommunications at the École Nationale d'Ingénieurs de Tunis, Tunisia.

From 1993 to 1997, he worked as a Research Engineer at the École Supérieure des Communications de Tunis, Tunisia, on switching systems and wireless channel characterization. Since 1998, he has been on a Ph.D. leave at INRS-Telecommunications, University of Quebec, Montreal, Canada. His current research interests include antenna-array receivers for third-generation wireless systems.

Sofiène Affes (S'94–M'95) received the Diplôme d'Ingénieur in electrical engineering, in 1992, and the Ph.D. degree in signal and image processing, in 1995, both from the École Nationale Supérieure des Télécommunications, Paris, France.

He was with INRS-Telecommunications, University of Quebec, Montreal, Canada, as a Research Associate from 1995 to 1997, then as an Assistant Professor until 2000. Currently he is an Associate Professor in the Personal Communications Group. His research interests include statistical signal and array processing, synchronization, and multiuser detection in wireless communications. Previously, he was involved in the European ESPRIT projects 2101 ARS on speech recognition in adverse environments in 1991 and 6166 FREETEL on hands-free telephony from 1993 to 1994. In 1997, he participated in the major program in personal and mobile communications of the Canadian Institute for Telecommunications Research. Since 1998, he has been leading the radio-design and signal processing activities of the Bell/Nortel/NSERC Industrial Research Chair in Personal Communications at INRS-Telecommunications.

Paul Mermelstein (S'58–M'63–SM'77–F'94) received the B.Eng. degree in engineering physics from McGill University, Montreal, Canada, in 1959, and the S.M., E.E., and D.Sc. degrees in electrical engineering from the Massachusetts Institute of Technology, Cambridge, MA, in 1960, 1963, and 1964, respectively.

From 1964 to 1973, he was a member of the Technical Staff in the Speech and Communications Research Department of Bell Laboratories, Murray Hill, NJ. From 1973 to 1977, he was a member of the Research Staff at Haskins Laboratories, conducting research in speech analysis, perception, and recognition. From 1977 to 1994, he was with Bell Northern Research, in a variety of management positions leading research and development activities in speech recognition, speech coding, and personal communications. From 1994 to 2000, he was the leader of the major program in personal and mobile communications of the Canadian Institute for Telecommunications Research. He holds the Bell/Nortel/NSERC Industrial Research Chair in Personal Communications at INRS-Telecommunications, University of Quebec, Montreal, Canada.

Dr. Mermelstein is a past Associate Editor for Speech Processing of the *Journal of the Acoustical Society of America* and Editor for Speech Communications of the IEEE TRANSACTIONS ON COMMUNICATIONS.